

# Cooperative effects of lattice and spin-orbit coupling on the electronic structure of orthorhombic $\text{SrIrO}_3$

Vijeta Singh<sup>1,2</sup> and J J Pulikkotil<sup>1,2,3</sup>

<sup>1</sup>Quantum Phenomena & Applications Division, CSIR-National Physical Laboratory, New Delhi 110012

<sup>2</sup>Academy of Scientific & Innovative Research (AcSIR), CSIR-National Physical Laboratory, New Delhi 110012

<sup>3</sup>Computation and Network Facility, CSIR-National Physical Laboratory, New Delhi 110012

E-mail: vijetasingh@nplindia.org, jiji@nplindia.org

**Abstract.** Orthorhombic  $\text{SrIrO}_3$  subjected to strain show tunable transport properties. With underlying symmetry remaining invariant, these properties are associated with  $\text{IrO}_6$  octahedral tilting. Adopting to first-principles methods, the effects of crystal field, spin-orbit coupling, and Coulomb correlations, on comparable interaction length scales, are discussed. While tilting induces a  $t_{2g} - e_g$  crystal-field splitting and band narrowing, spin-orbit coupling induces a partial splitting of the  $J_{eff}$  bands rendering  $\text{SrIrO}_3$  a semi-metallic ground state. The SOC enhanced hybridization of Ir-O orbitals, serve as a explanation to why the critical Hubbard correlation strength increases with increasing SOC strength in  $\text{SrIrO}_3$  to induce an insulating phase.

*Keywords:* Iridates, spin-orbit coupling, first-principles methods

Submitted to: *J. Phys.: Condens. Matter*

## 1. Introduction

In the Ruddlesden-Popper series  $\text{Sr}_{n+1}\text{Ir}_n\text{O}_{3n+1}$ ,  $n = 1$  ( $\text{Sr}_2\text{IrO}_4$ ) [1–6] and  $n = 2$  ( $\text{Sr}_3\text{Ir}_2\text{O}_7$ ) [6–10] are insulators, while  $n = \infty$ , ( $\text{SrIrO}_3$ ) is semi-metallic [11–13]. All systems in this series, chemically associate Ir with a formal valence of +4, due to its octahedral coordination ( $\text{IrO}_6$ ) with the neighboring ligands. The insulating ground state of  $\text{Sr}_2\text{IrO}_4$  and  $\text{Sr}_3\text{Ir}_2\text{O}_7$ , with Ir in its  $5d^5$  electronic configuration, is accounted by means of the spin-orbit coupling (SOC) driven  $J_{eff}$  model. According to the model, the  $t_{2g}$  bands in  $\text{Sr}_2\text{IrO}_4$  and  $\text{Sr}_3\text{Ir}_2\text{O}_7$  are split into  $J_{eff} = \frac{3}{2}$  and  $J_{eff} = \frac{1}{2}$  multiplets [1, 4, 14–17]. The  $J_{eff} = \frac{3}{2}$  states accommodate four electrons and therefore, are completely filled. The remaining electron is occupied into the  $J_{eff} = \frac{1}{2}$  doublet state. However, by virtue of their narrow bandwidth Coulomb correlations set in, which splits the  $J_{eff} = \frac{1}{2}$  doublets into two energetically distinct Hubbard bands, thereby, leading to an insulating ground state [18–23].

Interestingly, despite having a octahedral coordination with a formal  $\text{Ir}^{4+}$  state,  $\text{SrIrO}_3$  has a semi-metallic ground state. Fundamentally, this may be attributed to the underlying crystal structure, itself. Both  $\text{Sr}_2\text{IrO}_4$  and  $\text{Sr}_3\text{Ir}_2\text{O}_7$  crystallizes in tetragonal structure in which the  $\text{IrO}_6$  motifs are stacked along the crystallographic  $c$ -axis, separated by Sr ions. The  $\text{IrO}_6$  octahedra are distorted and tilted about the  $c$ -axis by an angle  $11^\circ$  in  $\text{Sr}_2\text{IrO}_4$  and  $12^\circ$  in  $\text{Sr}_3\text{Ir}_2\text{O}_7$  [9, 24, 25]. Since there is no direct linking of the these motifs along the  $c$ -axis, both  $\text{Sr}_2\text{IrO}_4$  and  $\text{Sr}_3\text{Ir}_2\text{O}_7$  display a quasi-two dimensional structure, commonly referred as single layered and bi-layered iridates, respectively. On the other hand,  $\text{SrIrO}_3$  crystallizes in both monoclinic and orthorhombic phases [26–28], with the former being the ambient phase. The orthorhombic structure is stabilized when synthesis conditions are adopted to high pressure and/or when grown in thin film form on appropriate substrates [11, 29–34]. In both monoclinic and orthorhombic phases, the  $\text{IrO}_6$  motifs of  $\text{SrIrO}_3$  are interlinked along all three crystallographic axes, thereby imparting a three dimensionality to its structure. Thus, unlike  $\text{Sr}_2\text{IrO}_4$  and  $\text{Sr}_3\text{Ir}_2\text{O}_7$ , there exists an additional Ir-O-Ir chemical bonding in  $\text{SrIrO}_3$ . Due to the additional structural constraint of the ions imposed by the  $c$ -axial bonding in  $\text{SrIrO}_3$ , the  $\text{IrO}_6$  octahedral tilt is enhanced to  $16^\circ$  [28], partly accounting the steric displacement of the Sr ions.

Octahedral distortions in perovskites are generally associated with size mismatch of the constituents and the nature of chemical bonding. Such distortions are manifested as tilting and/or elongation of the octahedra. Elongation usually results due to the dominant breathing modes which originate due to charge disappropriation in the system, as like in  $\text{BaBiO}_3$  where Bi exists in both +3 and +5 valence states. However, multiple valence states associated with Ir in  $\text{SrIrO}_3$  seems less likely, and thus octahedral tilting modes appear more dominant. Therefore, the energetics associated with the structure of  $\text{SrIrO}_3$  can be associated with the tilting of the  $\text{IrO}_6$  octahedra. Identifying the  $\text{IrO}_6$  octahedral tilt angle ( $\phi$ ) as a physical parameter, we study the electronic structure properties of  $\text{SrIrO}_3$  using first-principles density functional theory based methods. We find that octahedral tilting not only induce a  $t_{2g} - e_g$  crystal field splitting but also leads to significant band narrowing. Further, one finds that inclusion of SOC in the crystal Hamiltonian effectively splits the low energy antibonding states into  $J_{eff}$  states which are strongly hybridized. The calculations predict a semi-metallic ground state, which are consistent with the experimental observations. Also, following the empirical rigid band model of the alloy theory, it is anticipated that the transport properties of  $\text{SrIrO}_3$  would sensitively depend on the concentration of charge carriers, as well. Furthermore, adopting to Hubbard Hamiltonian, our calculations also show that Coulomb correlations in  $\text{SrIrO}_3$  have marginal effects on its low temperature electronic structure properties.

## 2. Computational details

Optimization of the structural parameters and the electronic structure properties of  $\text{SrIrO}_3$  are carried out using the full potential linearized augmented plane-wave (FP-LAPW) method as implemented in the Wien2k code [35]. The LAPW sphere radii for Sr, Ir and O were chosen as 2.26, 2.10 and 1.70 a.u., respectively. The lattice parameters were adopted to the experimental values, with  $a = 5.591$  Å,  $b = 5.561$  Å and  $c = 7.882$  Å [28]. The internal ionic coordinates of the Sr and O ions, which are not fixed by the symmetry, are relaxed using the force minimization technique. Well-converged basis sets were ensured, by choosing the Wien2k parameters  $RK_{max} = 8$ ;  $G_{max} = 24$  and  $l_{max} = 10$ . Additional local orbitals were also used to account for the semi-core Ir 5p states. The exchange correlation potential to the crystal Hamiltonian was considered in the generalized gradient approximation (GGA) as prescribed by Perdew, Burke and Ernzerhof [36]. The Brillouin zone  $k$ -mesh sampling for total energy convergence was modeled with 384  $k$ -points in its irreducible part. The core states were treated relativistically, while SOC was included for the valence states through the second variational step [37].

## 3. Results and discussions

### 3.1. Structure

	Sr		O(1)		O(2)		
	$x$	$z$	$x$	$z$	$x$	$y$	$z$
Expt	0.0420	0.9928	0.4812	0.07891	0.7965	0.9602	0.7965
Theory	0.0422	0.9927	0.4784	0.08107	0.7950	0.9585	0.7955
Bond distance (Å)		Bond angles ( $^\circ$ )					
	Ir-O(1)	Ir-O(2)	Ir-O(1)-Ir	Ir-O(2)-Ir			
Expt	2.0215	2.0281	154.205	152.491			
Theory	2.0251	2.0303	153.346	152.399			

**Table 1.** The GGA optimized structural parameters of  $\text{SrIrO}_3$  - the ionic coordinates, selected neighboring bond distances and bond angles, compared with the experiments [28].

To estimate the internal coordinates of Sr and O ions, force optimization was performed with its tolerance set to 1 mRy/a.u. The resulting structural parameters are found in good agreement with the experimental data [28]. The theoretical and experimental values are compared in Table 1.

The total energy minimization were also carried out by varying  $\phi$  to ascertain whether SOC has any prominent role in determining the structural properties of  $\text{SrIrO}_3$ . The values of  $\phi$  corresponding to these non-equilibrium structures, were estimated by using the relation  $\cos\theta_1 = \frac{(2-5\cos^2\phi_1)}{(2+\cos^2\phi_1)}$  and  $\cos\theta_2 = \frac{(1-4\cos^2\phi_2)}{2}$ . Here,  $\theta_1$  and  $\theta_2$  are the Ir-O(1)-Ir and Ir-O(2)-Ir bond angles with O(1) and O(2) representing the out-of-plane and in-plane O ions of the orthorhombic unit-cell. The average of  $\phi_1$  and  $\phi_2$  ( $\equiv \phi$ ) was used as the parameter to minimize the total energy. The variation in the total energy of  $\text{SrIrO}_3$  with respect to tilt angle,  $E(\phi)$ , is shown in Fig.1. Compared to the experimental value of  $15.8^\circ$ , we find that the scalar relativistic GGA calculations overestimate the equilibrium  $\phi$  as  $16.5^\circ$ , while the GGA+SOC calculations underestimate it to  $15.2^\circ$ .

The origin of octahedral tilting in perovskites is mainly attributed to steric and/or electronic interactions. In the steric models, tilting is facilitated due to the misfit size of the cation. Following

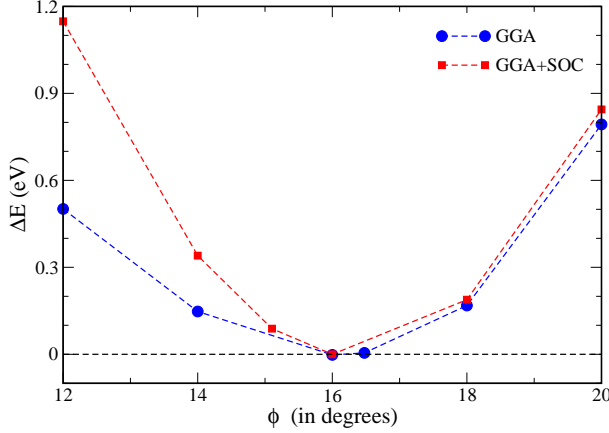


**Figure 1.** Color online : The relative change in the total energy, with respect to the equilibrium, as a function of  $\phi$  in  $\text{SrIrO}_3$ , calculated in the scalar relativistic GGA scheme ( blue line) and with SOC (red line) included in the Hamiltonian.

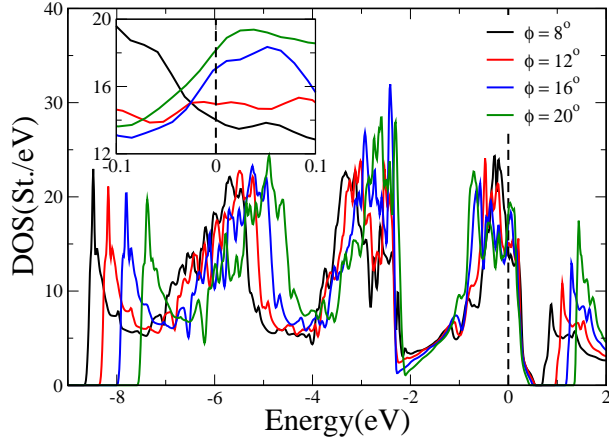
the GGA and GGA+SOC total energy calculations, the difference in the estimated equilibrium value of  $\phi$  differs more than  $1^\circ$ . Also, from Fig.1 it follows that the stiffness of the tilting, a quantity which is proportional to the second derivative of  $E(\phi)$  curve at equilibrium, increases substantially with SOC. The estimated increase with respect to scalar relativistic calculations is approximately three times larger. Therefore, it may be conjectured from these results that the large energy values associated with the structural perturbations may be of electronic in origin, rather than due to steric interaction, alone. Note that the energy associated with steric displacements of cations in oxide perovskites are usually of the order of few meV ( $\simeq 10 - 500$  K).

### 3.2. Electronic structure

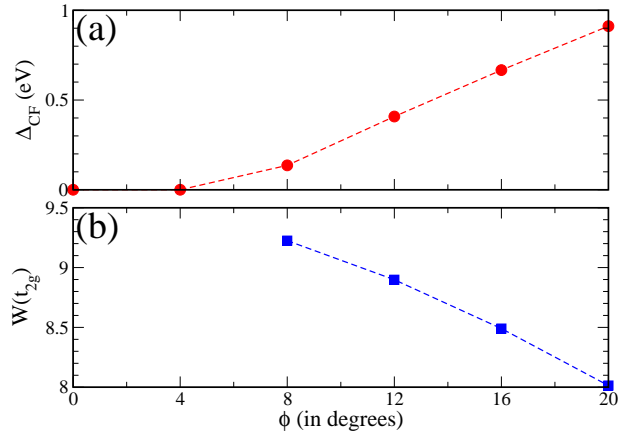
**3.2.1. Scalar relativistic calculations** To study, how the crystal field splitting ( $\Delta_{CF}$ ) of the  $t_{2g} - e_g$  bands evolve as a function of  $\phi$ , we show in Fig.2, the density of states (DOS) of  $\text{SrIrO}_3$ , for  $8^\circ \leq \phi \leq 20^\circ$ . For  $\phi \leq 4^\circ$ , the  $t_{2g}$  and  $e_g$  states are strongly hybridized and results in no electronic gap between them. A crystal field induced gap emerges for  $\phi > 4^\circ$ , the magnitude of which linearly increases with  $\phi$ , as shown in the Fig.3(a). The  $\Delta_{CF}$  gap resides in the unoccupied part of the DOS spectra. The integrated DOS from  $E_F$  to the top of the  $t_{2g}$  band is estimated as  $\simeq 1e^-$  per formula unit, consistent with the  $5d^5$  configuration of Ir ions in  $\text{SrIrO}_3$ .

Fig.2 also reveals significant  $t_{2g}$  band narrowing with increasing  $\phi$ . The bottom of the Ir 5d valence band at  $\simeq -9$  eV below  $E_F$  for  $\phi = 0^\circ$  linearly shifts to lower binding energies with increasing  $\phi$ , and is estimated to be at  $-7.5$  eV for  $\phi \simeq 20^\circ$ . Nevertheless, the top of the  $t_{2g}$  band at  $\simeq 0.6$  eV above  $E_F$  appears to be more or less pinned, irrespective of  $\phi$ , for  $\phi > 4^\circ$ . The variation in the  $t_{2g}$  bandwidth,  $W(t_{2g})$ , as a function of  $\phi$  is shown in Fig.3(b). For the equilibrium structure, the  $t_{2g} - e_g$  crystal field splitting was estimated as  $\simeq 0.55$  eV. Thus,  $\text{IrO}_6$  octahedra tilting not only induce a  $t_{2g} - e_g$  crystal field splitting in  $\text{SrIrO}_3$ , but also lead to a significant  $t_{2g}$  band narrowing of the Ir 5d manifold.

The atom resolved partial DOS of  $\text{SrIrO}_3$  (*not shown*) also reveal a wide spread distribution of the Ir 5d and O 2p states over the entire energy region, suggesting a covalent nature of chemical



**Figure 2.** Color online: The GGA derived DOS of  $\text{SrIrO}_3$  calculated with various  $\text{IrO}_6$  tilt angles, as indicated by the legends. The inset shows the blow-up of the states near  $E_F$  and the Fermi level. A vertical line (black) through energy zero represents the



**Figure 3.** Color online: (a) The change in the magnitude of the  $t_{2g} - e_g$  crystal field splitting of the Ir  $5d$  manifold and (b) the decreasing  $t_{2g}$  band width as a function of the  $\text{IrO}_6$  tilt angle,  $\phi$  in  $\text{SrIrO}_3$ , calculated using the GGA formalism of electronic structure method.

bonding in  $\text{SrIrO}_3$ . Both bonding and antibonding states are evident in the valence band spectra, which are separated by a pseudo-gap like feature at  $-2.3$  eV below  $E_F$ , i.e., the states in the energy range  $-8 \leq E(\text{eV}) \leq -2.3$  represent the bonding states, while those above  $-2.3$  eV constitute the antibonding states. One may note from Fig.2 that the relative energy position of the bonding - antibonding states in  $\text{SrIrO}_3$  and all non-equilibrium structures appear to be fixed, irrespective of the  $\text{IrO}_6$  octahedral tilt angle.

The GGA DOS find  $E_F$  on the higher side of the  $t_{2g}$  band, with  $\simeq 4.25$  St./eV/f.u., indicating  $\text{SrIrO}_3$  to be a good metal. However, this is in sharp contrast with the experiments which characterize  $\text{SrIrO}_3$  as a semi-metal. Furthermore, within the realms of Stoner theory of itinerant

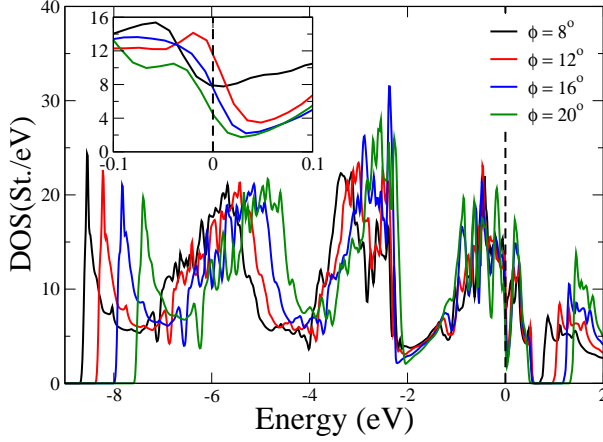


**Figure 4.** Color online : The GGA+SOC derived DOS of  $\text{SrIrO}_3$  as a function of  $\text{IrO}_6$  tilt angle  $\phi$ , the magnitude of which are indicated by the legends. The inset shows the blow-up of the states near  $E_F$ . The vertical broken line through energy zero represents the Fermi energy.

magnetism such high DOS at Fermi energy,  $N(E_F)$ , infers to a magnetic instability. The Stoner product,  $N(E_F) \times I$ , where  $I$  is the Stoner factor is estimated as 1.2 in  $\text{SrIrO}_3$ , with  $I(\text{Ir}) \simeq 0.574$  [38]. Following these predictions from the GGA calculations, we carried out spin polarized calculations. A ferromagnetic (FM) solution was found with Ir local magnetic moment being  $0.13 \mu_B$ , which was largely associated with the splitting of the  $t_{2g}$  anti-bonding states. Beyond, the GGA total energy difference between the non-magnetic and ferromagnetic states was found to be nearly degenerate. The prediction of magnetic ordering in  $\text{SrIrO}_3$ , following GGA calculations is in contradiction with the experiments which find no long range magnetic ordering in  $\text{SrIrO}_3$ . Furthermore, we also extended our calculations to check for any stable antiferromagnetic solution with initial Ir spin configuration assigned in the antiferromagnetic A-type, C-type and G-type structures. However, all these calculations converged to a non-magnetic solution. These results, therefore, indicate that the scalar relativistic Hamiltonian although accounts for the crystal field gap and  $t_{2g}$  band narrowing in  $\text{SrIrO}_3$ , however, fails to account for the distribution of electronic states, in particular, that of the near  $E_F$  anti-bonding states.

**3.2.2. Effects of spin-orbit coupling** Given that SOC becomes increasingly important for  $5d$  elements, we show in Fig.4, the DOS computed by means of the GGA+SOC calculations. The overall features of the DOS spectra in the bonding region looks similar to that of the scalar relativistic calculations, while the antibonding states appear to be strongly perturbed. Comparison of Fig.2 and Fig.4 reveals that the energy distribution of the states in the vicinity of  $E_F$ , *i.e.*,  $-0.5 \leq E \leq +0.5$ , undergo a drastic redistribution with a valley like feature emerging with its depth increasing concomitantly with  $\phi$ . For the equilibrium structure ( $\phi \simeq 16^\circ$ ) the  $N(E_F)$  reduces to 1.88 St./eV/f.u., which is significantly smaller in comparison with the scalar relativistic result. The reduction in  $N(E_F)$  is primarily due to the partial splitting of the  $J_{eff}$  states of the Ir  $t_{2g}$  manifold. According to the  $J_{eff}$  model of iridates, SOC splits the Ir  $t_{2g}$  states into  $J_{eff} = \frac{1}{2}$  and  $J_{eff} = \frac{3}{2}$  states. If one associates the Ir formal chemical valence in  $\text{SrIrO}_3$  as +4, simple band filling assuming an ionic picture, would suggest that the low energy  $J_{eff} = \frac{3}{2}$  states which are a linear combination

of  $|m_j|=\frac{1}{2}$  and  $|m_j|=\frac{3}{2}$  states would occupy two electrons each leaving  $J_{eff} = \frac{1}{2}$  doublet singly occupied. The integrated DOS from  $E_F$  to the top of the  $t_{2g}$  band in SrIrO<sub>3</sub> yields  $\simeq 1$   $e^-$  per formula unit. However, quite different from the case of insulating Sr<sub>2</sub>IrO<sub>4</sub> and Sr<sub>3</sub>Ir<sub>2</sub>O<sub>7</sub>, the  $J_{eff}$  states in SrIrO<sub>3</sub> are found to be a superposition of both  $J_{eff} = \frac{1}{2}$  and  $J_{eff} = \frac{3}{2}$  states yielding a semi-metallic ground state. We note that the hybridization of  $J_{eff} = \frac{1}{2}$  and  $J_{eff} = \frac{3}{2}$  states in SrIrO<sub>3</sub>, more or less follows from the three dimensionality of its structure, due to which both in-plane and out-of-plane O  $2p$  orbitals have considerable overlap with the Ir  $5d$  orbitals. Note that in Sr<sub>2</sub>IrO<sub>4</sub> and Sr<sub>3</sub>Ir<sub>2</sub>O<sub>7</sub>, there is no orbital overlap of the Ir  $5d$  orbitals with the out-of-plane O ions, primarily due to their quasi two dimensional structure.

We also find a strong dependence of  $N(E_F)$  with  $\phi$ . For example, the  $N(E_F)$  reduces to 1.06 St./eV/f.u for  $\phi = 20^\circ$  while, for reduced tilting  $\phi = 12^\circ$  it increases to 2.39 St./eV/f.u. Apart from the decrease in  $N(E_F)$  with increasing  $\phi$ , we also find that the energy derivative of DOS at  $E_F$  also increases. The latter implies to an increase in the effective mass or in other words, a decrease in carrier mobility ( $\mu$ ). Overall, the GGA+SOC calculations which find a decrease, both in  $N(E_F)$  and  $\mu$  with structural perturbations clearly suggest that the transport properties of SrIrO<sub>3</sub> can be controlled by tilting the octahedra, which in turn can be accomplished by strain. This is consistent with the strain dependent studies of orthorhombic SrIrO<sub>3</sub> films grown on different substrates. Tunable semi-metallic and metal-insulator transitions have been observed in experiments due to lattice mismatch of the orthorhombic SrIrO<sub>3</sub> with that of the substrates [30, 31]. It is inferred from the experiments that in-plane compressive strain decreases the Ir  $5d$  bandwidth. With the underlying symmetry of the lattice being unchanged, it can therefore be well anticipated that the increase in the energy of the system due to strain would be minimized mainly via the displacement of O ions, implying IrO<sub>6</sub> octahedral tilting.

Moreover, in the context that octahedral tilting in SrIrO<sub>3</sub> leads to the  $t_{2g}$ - $e_g$  band splitting and narrowing of the bands, then conversely, SOC via structural modifications enhance the extent of Ir  $5d$  and O  $2p$  orbital overlap. The argument follows from the fact that GGA when finds the equilibrium  $\phi$  as  $16.5^\circ$ , GGA+SOC estimates it to  $15.2^\circ$ . Therefore, enhanced hybridization of Ir  $5d$  - O  $2p$  orbitals would reflect to an enhanced dispersion of these hybridized bands. Based on the hybridization and Coulomb correlations analogy, our argument is consistent with the fact that increased SOC enhance the critical Hubbard interaction strength to drive an insulating ground state in SrIrO<sub>3</sub> [39].

**3.2.3. Role of carrier concentration** Having found that the structure and spin-orbit coupling play an important role in determining the electronic structure of SrIrO<sub>3</sub>, we investigate the role of carrier concentration in SrIrO<sub>3</sub>. The blow-up of near  $E_F$  region, as shown in Fig.4, shows that the position of  $E_F$  is not at the bottom of the valley, but resides along its negative slope. Therefore, based on the rigid band model of electronic structure it could be anticipated that electron doping, which can be accomplished via O defects, would slide the  $E_F$  down the valley, thereby decreasing  $N(E_F)$  further. In general, a low  $N(E_F)$  also indicate to higher phase stability. Therefore, such O defects modified electronic structure appears quite favorable in SrIrO<sub>3</sub>, which along with structural perturbations would increase the propensity of the system to exhibit metal-insulator transitions.

The carrier concentration in SrIrO<sub>3</sub> is estimated to be  $\sim 10^{20}$   $e/cm^3$  [34], the magnitude of which lies in the vicinity of the semiconductor – metal phase boundary of the solid state. In the rigid band model, accommodating  $10^{20}$   $e/cm^3$  ( $\equiv 0.0245$   $e/u.c.$ ) in the DOS spectra necessitate a shift of  $E_F$  by 23 meV. Such an effect significantly reduce  $N(E_F)$  to 0.82 St./eV/u.c., thereby increasing the propensity of a metal-insulator transition in SrIrO<sub>3</sub>. Moreover, for an enhanced IrO<sub>6</sub>

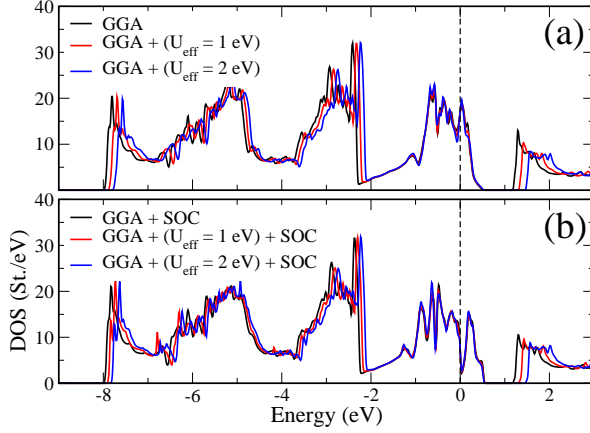


**Figure 5.** Color online : The calculated DOS using the GGA+ $U_{eff}$  scheme (a) without and, (b) with SOC, for the equilibrium structure ;  $\phi \simeq 16^\circ$ . The vertical broken line through energy zero represents the Fermi energy.

tilting, say  $\phi = 20^\circ$ , a carrier concentration corresponding to  $10^{20} \text{ e/cm}^3$  yields a of  $N(E_F)$  0.30 St./eV/u.c. Thus, we find that cooperative effects associated with octahedral tilting, SOC and carrier concentration in  $\text{SrIrO}_3$  play an important role in controlling the transport properties of the system.

**3.2.4. Effects of Coulomb correlations** We also have studied the effect of Coulomb correlations on the electronic structure of  $\text{SrIrO}_3$ . In Fig.5(a), we compare the GGA and GGA+ $U_{eff}$  DOS. Evidently, the most notable effect with Coulomb correlations in  $\text{SrIrO}_3$  is the increase in the magnitude of the crystal field gap between the  $t_{2g}$  and  $e_g$  bands. Also, while a small shift on the energy scale is also observed for the bonding states, the distribution of electronic states in the antibonding states remains more or less unchanged. On the other hand, the GGA+ $U_{eff}$ +SOC calculations, the results of which are shown in Fig.5(b), reveal no significant changes in the electronic structure arising due to Coulomb correlations. Thus, on a comparative length scale (0.5 - 2 eV) between the crystal field splitting, SOC and Coulomb correlations, the effect on Coulomb correlations on the electronic structure appears to be very marginal.

Moreover, to study how Coulomb correlations and SOC compete in  $\text{SrIrO}_3$ , we carried out spin polarized calculations in the GGA+ $U_{eff}$  scheme for  $0 \leq U_{eff} \text{ (eV)} \leq 4 \text{ eV}$ . In these calculations, an Ir local magnetic moment was computed in the FM and AFM-A and AFM-G structures, for all values of  $U_{eff}$ . For the AFM-C type ordering, an Ir local moment appeared only when  $U_{eff} > 3.5 \text{ eV}$ . Note that the emergence of magnetic moment at the Ir sites with  $U_{eff}$  can be attributed to the increased localization of the  $5d$  states. However, with inclusion of SOC term in the Hamiltonian, all calculations with  $U_{eff} < 3.5 \text{ eV}$ , irrespective of the underlying magnetic ordering, converged to nonmagnetic solution. Since the origin of local moments in the GGA+ $U_{eff}$  are associated with localization of the  $5d$  states, its annihilation with SOC for  $U_{eff} < 3.5 \text{ eV}$  is to be attributed to the delocalization (or enhanced hybridization) of the corresponding states with O  $2p$  orbitals. However, we note that a stable magnetic moment ( $\simeq 0.5 \mu_B$ ) was found for all magnetic structures in the GGA+ $U_{eff}$ +SOC scheme of calculations when  $U_{eff} > 3.5 \text{ eV}$ , *i.e.*, when the magnitude of  $U_{eff}$



exceeds the Ir  $5d$  bandwidth. Based on these calculations, we argue that on a comparable length scale of interactions, Coulomb correlations and SOC compete with each other, with SOC partly nullifying the Ir  $5d$  localization effects by enhancing the inter-atomic Ir and O orbital hybridization.

#### 4. Summary and conclusion

In summary, we find a cooperative effect on the electronic structure of  $\text{SrIrO}_3$  due to an interplay of its underlying lattice and SOC. Octahedral tilting of the  $\text{IrO}_6$  motif in  $\text{SrIrO}_3$  appears to be primary source of crystal field splitting of the  $t_{2g} - e_g$  bands. The magnitude of the splitting scales with tilt angle, which also results in band narrowing. On the other hand, SOC induces a partial splitting of the  $t_{2g}$  bands into  $J_{eff}$  states which reduce  $N(E_F)$ , driving  $\text{SrIrO}_3$  to a semi-metallic ground state. Taking into consideration that the tilt angle can be tuned by strain and that electron doping can be accomplished via controlled O defects, the propensity to drive in a metal-insulator transition in  $\text{SrIrO}_3$  appears consistent with the experiments. Besides, on a comparative length scale of interactions, we find that the effect of Coulomb correlations on the electronic structure of  $\text{SrIrO}_3$  is very nominal. Interestingly, the SOC enhanced orbital hybridization also substantiates the preposition that the magnitude of the critical Hubbard interaction strength to drive an insulating ground state in  $\text{SrIrO}_3$ , increases with increasing SOC strength.

#### Acknowledgments

The authors thank A. K. Shukla for helpful discussions. VS acknowledges CSIR, India for JRF fellowship and JJP acknowledges financial assistance from the CSIR XII FYP project, AQUARIUS.

#### References

- [1] B. J. Kim, H. Ohsumi, T. Komesu, S. Sakai, T. Morita, H. Takagi, and T. Arima, *Science* 323, 1329 (2009).
- [2] N. S. Kini, A. M. Strydom, H. S. Jeevan, C. Geibel, and S. Ramakrishnan, *J. Phys.: Condens. Matter* 18, 8205 (2006).
- [3] M. K. Crawford, M. A. Subramanian, R. L. Harlow, J. A. Fernandez-Baca, Z. R. Wang, and D. C. Johnston, *Phys. Rev. B* 49, 9198 (1994).
- [4] G. Cao, J. Bolivar, S. McCall, and J. E. Crow, and R. P. Guertin, *Phys. Rev. B* 57, R11039 (1998).
- [5] B M Wojek, M H Berntsen, S Boseggia, A T Boothroyd, D Prabhakaran, D F McMorro, H M Rønnow, J Chang and O Tjernberg, *J. Phys.: Condens. Matter* 24 415602 (2012).
- [6] D. A. Zocco, J. J. Hamlin, B. D. White, B. J. Kim, J. R. Jeffries, S. T. Weir, Y. K. Vohra, J. W. Allen, M. B. Maple, *J. Phys.: Condens. Matter* 26, 255603 (2014).
- [7] S. Boseggia, R. Springell, H. C. Walker, A. T. Boothroyd, D. Prabhakaran, S. P. Collins, and D. F. McMorro, *J. Phys.: Condens. Matter* 24 (2012).
- [8] P. D. C. King, T. Takayama, A. Tamai, E. Rozbicki, S. McKeown Walker, M. Shi, L. Patthey, R. G. Moore, D. Lu, K. M. Shen, H. Takagi, and F. Baumberger *Phys. Rev. B* 87, 241106(R) (2013).
- [9] M. A. Subramanian, M. K. Crawford and R. L. Harlow, *Mater. Res. Bull.* 29, 645 (1994).

- [10] I. Nagai, Y. Yoshida, S. I. Ikeda, H. Matsuhata, H. Kito, and M. Kosaka, *J. Phys. Condens Matter* 19 (2007).
- [11] Y. F. Nie, P. D. C. King, C. H. Kim, M. Uchida, H. I. Wei, B. D. Faeth and K. M. Shen, *Phys. Rev. Lett.* 114, 016401 (2015) .
- [12] S. J. Moon, H. Jin, K. W. Kim, W. S. Choi, Y. S. Lee, J. Yu and T. W. Noh, *Phys. Rev. Lett.* 101, 226402 (2008).
- [13] H. Zhang, K. Haule, and D. Vanderbilt, *Phys. Rev. Lett* 111, 246402 (2013).
- [14] S. Fujiyama, H. Ohsumi, T. Komesu, J. Matsuno, B. J. Kim, M. Takata and H. Takagi, *Phys. Rev. Lett.* 108, 247212 (2012).
- [15] B. J. Kim, H. Jin, S. J. Moon, J. Y. Kim, B. G. Park, C. S. Leem, J. Yu and E. Rotenberg, *Phys. Rev. Lett.* 101, 076402 (2008).
- [16] S. J. Moon, H. Jin, W. S. Choi, J. S. Lee, S. S. A. Seo, J. Yu and Y. S. Lee, *Phys. Rev. B* 80, 195110 (2009).
- [17] S. J. Moon, M. W. Kim, K. W. Kim, Y. S. Lee, J. Y. Kim, J. H. Park and T. W. Noh, *Phys. Rev. B* 74, 113104 (2006).
- [18] D. Pesin and L. Balents, *Nat. Phys.* 6, 376 (2010).
- [19] H. Watanabe, T. Shirakawa, and S. Yunoki, *Phys. Rev. Lett.* 105, 216410 (2010).
- [20] F. Wang and T. Senthil. *Phys. Rev. Lett.* 106, 136402 (2011).
- [21] G. Jackeli and G. Khaliullin, *Phys. Rev. Lett.* 102, 017205 (2009).
- [22] J. Chaloupka, G. Jackeli and G. Khaliullin. *Phys. Rev. Lett.* 105, 027204 (2010).
- [23] J. M. Carter, V. V. Shankar and H.-Y. Kee, *Phys. Rev. B* 88, 035111 (2013).
- [24] R. Arita, J. Kunes, A. V. Kozhevnikov, A. G. Eguiluz and M. Imada, *Phys. Rev. Lett.* 108, 086403 (2012).
- [25] Q. Huang, J. L. Soubeyroux, O. Chmaissem, I. N. Sora, A. Santoro, R. J. Cava and W. F. Peck, *J. Solid State Chem.* 112, 355(1994).
- [26] G. Cao, V. Durairaj, S. Chikara, L. E. DeLong, S. Parkin and P. Schlottmann, *Phys. Rev. B.* 76, 100402 (2007).
- [27] J. M. Longo, J. A. Kafalas and R. J. Arnett, *J. Solid State Chem.* 3, 174 (1971).
- [28] J. G. Zhao, L. X. Yang, Y. Yu, F. Y. Li, R. C. Yu, Z. Fang and C. Q. Jin, *J. Appl. Phys.* 103, 103706 (2008).
- [29] S. Y. Jang, H. Kim, S. J. Moon, W. S. Choi, B. C. Jeon, J. Yu and T. W. Noh, *J. Phys. Condens. Matter* 22, 485602 (2010).
- [30] J. H. Gruenewald, J. Nichols, J. Terzic, G. Cao, J. W. Brill, S. S. A. Seo, *J. Mater. Res.* 29, 2491 (2014).
- [31] L. Zhang, Q. Liang, Y. Xiong, B. Zhang, L. Gao, H. Li and Y. F. Chen, *Phys. Rev. B*, 91, 035110 (2015).
- [32] G. Cao, X. N. Lin, S. Chikara, V. Durairaj and E. Elhami, *Phys. Rev. B* 69, 174418 (2004).
- [33] F. X. Wu, J. Zhou, L. Y. Zhang, Y. B. Chen, S. T. Zhang, Z. B. Gu and Y. F. Chen, *J. Phys.: Condens. Matter* 25, 125604 (2013).
- [34] A. Biswas, K. S. Kim and Y. H. Jeong, *J. Appl. Phys.* 116, 213704 (2014).

- [35] P. Blaha, K. Schwarz, G. Madsen, D. Kvasicka, and J. Luitz, computer code WIEN2K, Technical University of Vienna, Vienna (2001).
- [36] J. P. Perdew, K. Burke and M. Ernzerhof, Phys. Rev. Lett. 77, 3865 (1996).
- [37] D. D. Koelling and B. N. Harmon, J. Phys. C 10, 3107 (1977)
- [38] A. E. Garcia, V. G. Robles and R. Baquero, Phys. Rev. B 59, 9392(1999).
- [39] M. A. Zeb, and H.-Y. Kee, Phys. Rev. B 86, 085149 (2012).